JOURNAL OF MATERIALS SCIENCE 33 (1998) 3407–3417

Axial compressive behaviour of reinforcing fibres and interphase in glass/epoxy composite materials

N. OYA, H. HAMADA
Faculty of Textile Science, Kyoto Institute of Technology, Matsugasaki, Sakyo-ku, Kyoto 606, Japan
E-mail: hhamada@ipc.kit.ac.jp

Axial compressive behaviour of reinforcing fibres and interphase in glass fibre/epoxy resin composites were examined. Axial compressive strengths of glass fibres were evaluated by the tensile recoil method. The effects of silane-based coupling surface treatment agent on the fibre compressive strengths were investigated. The glass fibres showed higher compressive strengths when coated by the surface treatment. Interphase behaviour was also investigated by means of the single-fibre embedded compressive test. The particular stress and strain distributions inside the specimen were examined by a three-dimensional finite element analysis. The parameter "*interfacial transmissibility*" instead of the conventional critical fibre length theory was introduced as an index of interfacial properties. This parameter was useful to estimate the interfacial properties at the elastic state apart from the complicated critical state. It was confirmed that the surface treatment improved the glass/epoxy interphase under axial compressive load. © *1998 Kluwer Academic Publishers*

1. Introduction

A current limitation to the broader usage of fibre-reinforced composite materials is associated with their inherently poor and complicated compressive behaviour along the reinforcing fibre axis. Many researchers have investigated their tensile behaviour; however, the compressive behaviour has not been sufficiently elucidated owing to the experimental difficulties. There has been an urgent demand for separate detailed investigations of the compressive behaviour of each component, fibre, matrix and interphase.

Several methods for the longitudinal compressive test of single fibres have so far been proposed. The main methods used are the elastic loop method [1–6], the matrix shrinkage method [7], the bending beam method [7–9], the single-fibre composite method [10–14] and the tensile recoil method [15–19]. Among these methods, the tensile recoil method has been regarded as the most reliable way to evaluate the axial compressive strengths of fine fibres.

The compressive behaviour of the interphase is particularly difficult to investigate. In fact, no method has been standardized or proposed at the moment. However, several methods have been developed for the tensile behaviour of the interphase by many researchers. They are the fibre pull-out method [20–22], the fibre push-in method [23–26] and the single-fibre embedded composite method [27–30]. The single-fibre embedded tensile test is widely used for this purpose because it does not need any sophisticated specimen preparation. In this method, the critical fibre length has been mainly measured to evaluate the interfacial shear strength [31–34]. Because tensile forces are transmitted to the fibre through the interphase and the strain-to-failure of the fibre is much lower than that of the matrix, the fibre will be fractured into small segments within the matrix. As higher tensile loads are applied, the fracture process continues until the interphase can no longer transfer sufficient forces to induce fibre fracture. At this point, a minimum segment length might be obtained as the critical fibre length.

There are some problems concerned with the determination of the critical fibre length [29, 35–37]. The first is that the critical state is difficult to define clearly. Secondly, the availability of a material system in which brittle fibre and ductile matrix must be used is limited. Thirdly, the calculation of the interfacial shear strength is based on the assumption of an ideally plastic matrix and constant interfacial shear stress over the fragment length. In fact, various kinds of interphase model will have to be considered at the critical state. Many researchers have reported significant progress in this field using sophisticated elastic/plastic analyses [38–40], finite element analyses [41–45] and even direct measurements of the stress distributions inside single-fibre embedded composites [46–51]. Nevertheless, because of the existence of interfacial debonding, the stress distribution at the critical state should be very complicated. It is desirable to evaluate the interphase during the elastic range. A breakthrough in this problem has been discussed by Hamada *et al.* [36], and details will be given later.

It would appear that it is also possible to apply the single-fibre composite technique under compressive force; however, the reality is not very optimistic. Not only the problem of the elastic range but also of fibre misalignments and specimen buckling must be carefully removed. Several researchers have succeeded in

observing compressive fractures of fibres and interfacial debonding within properly compressed single fibre composite specimens [10–14]; however, they have not been able to determine the interfacial properties. Detailed analysis of experimental results will also be needed in addition to the single-fibre embedded tensile test.

In this study, axial compressive properties of single glass fibres and the glass/epoxy interphase were determined by the tensile recoil test and an newly developed single-fibre embedded composite test, respectively. Results from the composite test were carefully examined by means of a three-dimensional finite element method.

2. Experimental procedure

2.1. Materials

2.1.1. Glass fibres

The glass fibres used in this study were E-glass fibres treated with γ-amino-propyltriethoxysilane (APS) surface treatment agent. It is well known that the silane coupling agent is particularly effective for the adhesion between glass fibre and epoxy resin. The concentration of APS agent was varied: 0 (blank), 0.1, 0.5 and 1.0 w %.

2.1.2. Epoxy resin

The matrix resin was a stoichiometric mixture of a diglycidyl ether of bisphenol-A (Epon 828, Shell Chemical Co. Ltd.) cured with 11 p.h.r. triethylenetetramine.

2.2. Tensile recoil test

Axial compressive strengths of single glass fibres were measured using the tensile recoil method developed by Allen [15]. In this method, a filament sample is pulled under tension in a universal testing machine (Autograph AG-500E, Shimadzu Co. Ltd). When a predetermined stress level is reached, the tensile loading is temporarily stopped and a recoil effect is initiated on the fibre by cutting at the midpoint. Consequently, the stored tensile strain energy is converted to kinetic energy by the cutting, and the wave front eventually reaches the clamp end of the fibre. Because the clamp is assumed to be sufficiently rigid, the kinetic energy is again converted to compressive strain energy. As the clamp, is assumed to be rigid, there is no energy loss of heat, sound, etc. Therefore, the recoil compressive stress induced by the strain energy should be equal to the tensile stress applied to the sample. If this recoil compressive stress exceeds the compressive strength of the fibre, compressive failure occurs. In the case of brittle materials such as glass fibres, the compressive failure is catastrophic and easily identified by the eye. When compressive failure of the fibre occurs, however, it is not possible to determine the actual compressive strength of that fibre because the applied stress could have exceeded the critical compressive strength by an unknown amount. To overcome this problem, Allen [15] and Wang *et al.* [18] calculated the recoil compressive strength as the average of each end point stress in which 100% survival and 100% failure (0% survival) is observed, respectively.

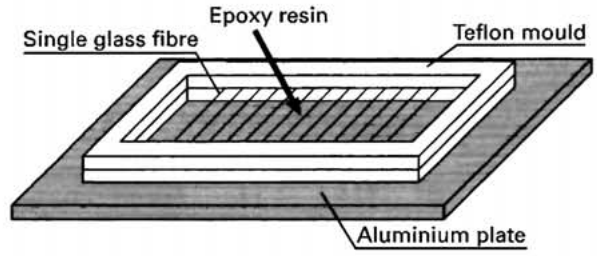

Figure 1 Single fibres embedded in epoxy resin.

2.3. Single-fibre embedded compressive test

Interphase behaviour under axial compression was examined by means of a single-fibre embedded compressive test. In the specimen preparation, glass fibres were embedded in an epoxy resin bath by gluing across a Teflon split mould on an aluminium plate, as shown in Fig. 1. Another aluminium plate was put on the mould and then the matrix system was processed for 80 min at 50 °C and 60 min at 100 °C followed by cooling overnight. After curing, the resin block was removed from the Teflon mould, and a circular-notched specimen, schematically shown in Fig. 2, was cut from the resin plate as the single fibre was embedded at the centre of the specimen. Top and bottom surfaces of each specimen were milled flat and parallel. Samples in which embedded single fibres were poorly aligned or otherwise unsuitable for testing, were discarded. Four kinds of APS-treated specimens were prepared (APS 0, 0.1, 0.5 and 1.0 wt %).

Samples were compressed between parallel anvils on an Instron universal testing machine (Type 4206, Instron Co. Ltd,) at 1 mm min^{-1} crosshead speed. Compressive loads were monitored using a load cell during the tests. Lateral supports by a compression jig recognized in ASTM D695 [52] were given to each specimen to prevent any buckling instabilities. All compressive tests were conducted at room temperature. After the compressive tests, changes or fracture aspects within the specimens were observed by optical microscopy.

3. Analytical methods

3.1. Interfacial transmissibility

As mentioned earlier in this paper, the uncertainty of the critical state in the single-fibre embedded tensile test is a problem. Hamada *et al.* [36] focused on the initial state of fibre fractures inside the specimen in order to avoid the drawback of the critical fibre length theory. They assumed a single-fibre composite model as shown in Fig. 3. It is defined that all the tensile load applied to the matrix is transmitted to the fibre through the interphase. If the fibre and matrix are completely bonded at the interphase, the strain applied on the matrix, ε_m, is completely transmitted to

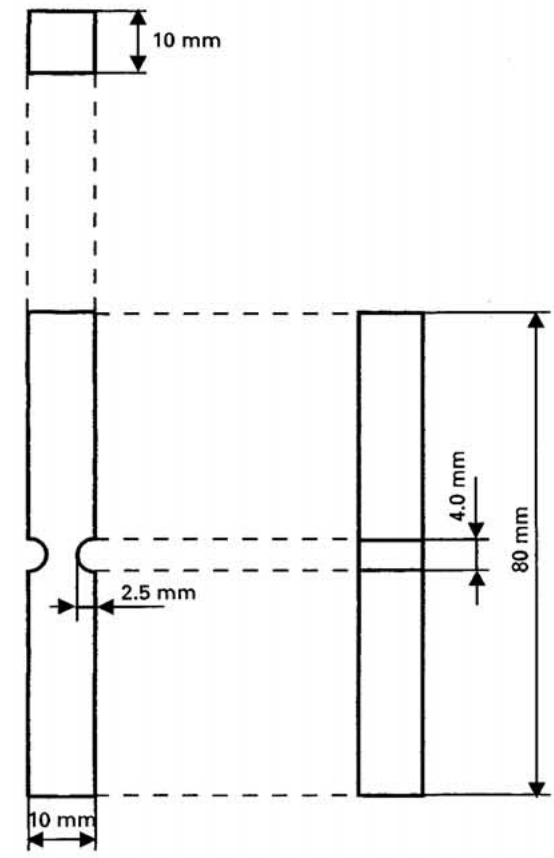

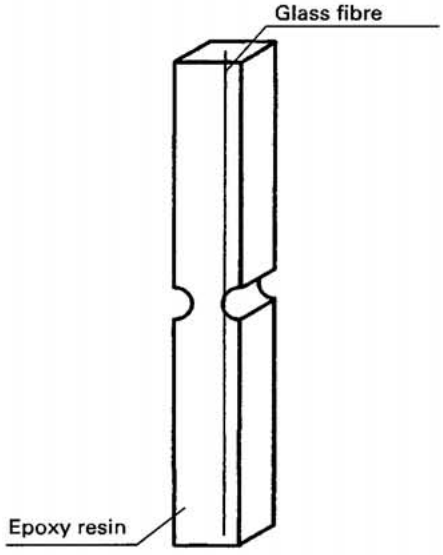

Figure 2 Specimen geometry for the single-fibre composite test.

the fibre and then the fibre strain, ε_f, is equal to the matrix strain

$$\varepsilon_f = \varepsilon_m = \varepsilon_c \quad (1)$$

where ε_c denotes the composite strain. However, the adhesion in an actual interphase is not perfect. The fibre strain usually becomes smaller than the applied strain in the matrix.

$$\varepsilon_f < \varepsilon_m = \varepsilon_c \quad (2)$$

Hence, the difference between ε_f and ε_m indicates the loss of strain at the interphase. The ratio of ε_f to ε_m, κ,

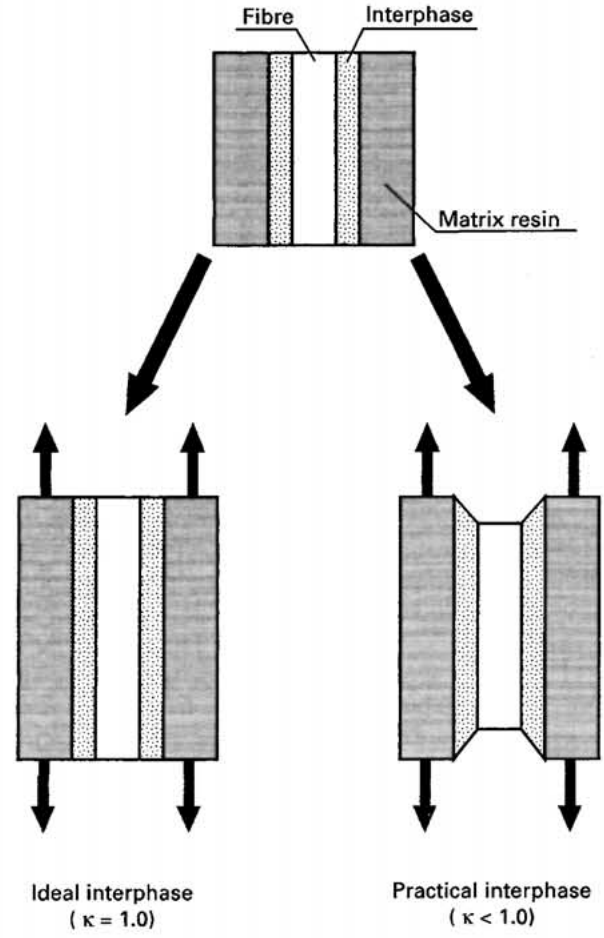

Figure 3 Concept of interfacial transmissibility.

can be regarded as a coefficient of strain transmissibility at the interphase

$$\kappa = \frac{\varepsilon_f}{\varepsilon_m} \quad (3)$$

In the ideal interphase system, $\kappa = 1$, and in practice less than 1. If the ultimate strain of the fibre and the matrix strain which corresponds to the first fibre fracture in the single-fibre embedded composite can be determined, κ can be evaluated as an index of interfacial property as the elastic stage. Using the parameter of interfacial transmissibility, the interphase property could be estimated in various systems, apart from the critical fibre length method.

However, the fibre strain within the composite specimen will be difficult to measure. The equation should be modified into Equation 4 by the Hookean law

$$\kappa = \frac{\sigma_f}{E_f \varepsilon_m} \quad (4)$$

where σ_f and E_f are compressive strength and elastic modulus of the fibre, respectively.

The interfacial transmissibility was successfully evaluated under the axial tensile load by Ikuta and co-workers [36, 53]. They used the results of single-fibre tensile tests for σ_f and E_f. ε_f was obtained from single-fibre embedded tensile tests as the specimen strain which corresponds to the first fibre fracture

detected inside. For application under axial compression, their method could be used by incorporating the results of the tensile recoil tests for σ_f and E_f should be identical to the tensile modulus because of the isotropic property of glass fibre. ε_m will be obtained from the single-fibre embedded compressive test.

3.2. Macro model

It was expected that the deformation state within the fibre-embedded specimen would be quite complex due to the circular notch shape. It is important to understand the strain state properly. The interior strain state was investigated by a finite element analysis. The whole shape of the specimen was modelled using three-dimensional solid elements in order to consider not only the axial compressive stress but also the transverse tensile stresses due to the Poisson's effect. The initial division of the "macro model" is presented in Fig. 4. A quarter of the actual specimen was modelled because of the symmetry. The total number of three-dimensional solid elements was 1540. The lateral support by the compression fixture was considered in the boundary conditions. Matrix resin properties were given to all the elements, considering the quite low fibre volume fraction (4.54×10^{-4}%).

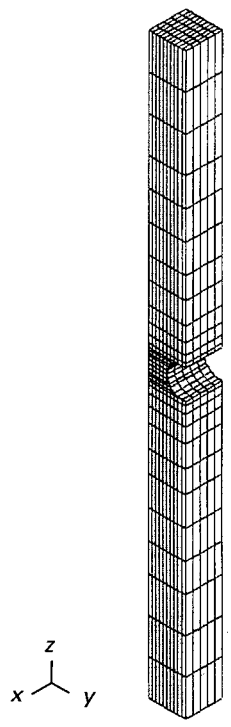

Figure 4 Finite element division of the macro model.

TABLE I Material properties of the macro model

Material	Element	Elastic modulus (GPa)	Poisson's ratio	Yield strength (MPa)
Epoxy resin	Isotropic 3D-solid	3.68 (before fracture) 0.55 (after fracture)	0.33	70.07

The material properties in the macro model are presented in Table I. In order to obtain these compressive properties of epoxy resin, static compressive tests were preliminarily conducted for rectangular resin plates with strain gauges attached. The yield strength was directly measured from the specimens and then the elastic moduli were estimated in both elastic and plastic ranges.

Non-linear analysis for the macro model was conducted by a displacement incremental method. The displacement was applied on the top of the macro model along the longitudinal, Z, direction. Strains were calculated in all elements at each displacement.

3.3. Micro model

The stress state inside or near the interphase was examined by another finite element model called the "micro model" which considers fibre, matrix and interphase. Finite element division of the micro model is shown in Fig. 5. The strain state of the central element in the macro model was used as input data for the micro model. Fibre, interphase and matrix resin were divided into three portions, namely the upper, intermediate and bottom parts, along the Z direction. The length was 10 μm for each element. The radius of the fibre element was 8.5 μm (from the catalogue value) and the thickness of the interphase element was assumed to be 1.5 μm. The particular thickness of the interphase was only supposed as a reasonable value in this system. The material properties in the micro model are presented in Table II. Under compression, apart from tension, the glass fibre is crushed at failure and subsequently compressed showing a lower elastic

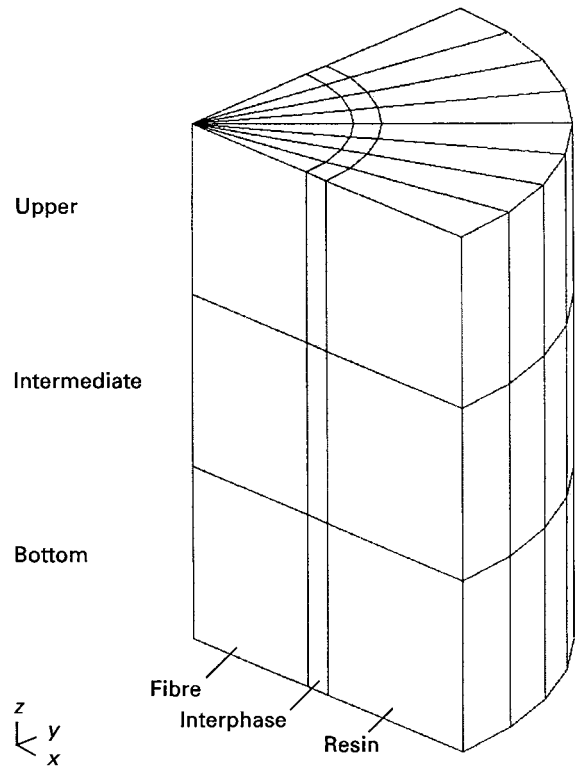

Figure 5 Finite element division of the micro model.

TABLE II Material properties of the micro model

Material	Element	Elastic modulus (GPa)	Poisson's ratio	Yield strength (MPa)
Glass fibre	Isotropic 3D-solid	70.00 (before fracture) 1.00 (after fracture)	0.22	Varied
Interphase	Isotropic 3D-solid	Varied (before fracture) 0 (after fracture)	0.33	Varied
Epoxy resin	Isotropic 3D-solid	3.68 (before fracture) 0.55 (after fracture)	0.33	70.07

TABLE III Compressive strengths of E-glass fibres

Surface treatment condition	Recoil strength (MPa)	0% failure (MPa)	100% failure (MPa)
No APS	1519	1468	1569
0.1 wt % APS	1919	1599	2239
0.5 wt % APS	1826	1727	1925
1.0 wt % APS	1922	1610	2233

modulus. Therefore, we assume that the glass fibre can yield. The elastic modulus of the interphase and strengths of the fibre and interphase were varied. Non-linear analysis for the micro model was conducted by a displacement incremental method as well as the macro model. The normal and shear stress components were calculated in all elements at each displacement.

4. Experimental results

4.1. Axial compressive strength of glass fibre

Recoil compressive strengths of glass fibres are listed in Table III with their range of strengths (0% and 100% failure stresses). APS-treated glass fibres showed higher compressive strengths compared with the non-treated fibre. These results were probably related to coating effects of the APS surface treatment agent. It is deduced that crack initiation from a fine flaw existing on the fibre surface tended to be prevented due to the coating effect.

4.2. Fracture behaviour inside single-fibre embedded compressive specimens

A typical compressive stress-displacement curve for the single-fibre embedded compressive specimen is shown in Fig. 6. It is seen that the slope of the curve decreased from the displacement of around 3 mm. This was due to plastic deformation of the matrix resin, and in fact the notched central portion swelled at that testing stage. However, the compressive stress subsequently increased after plastic deformation.

At a displacement of around 3 mm, the first fibre fracture occurred at the centre of the specimen. The

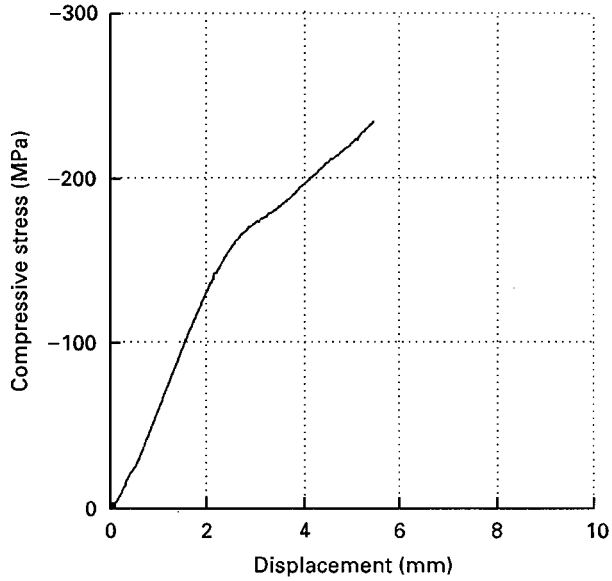

Figure 6 Typical compressive stress–displacement curve for single-fibre composite test.

number of fracture points increased and the location spread to either side of the centre with increase of compressive load. Moreover, the fracture aspect changed, as shown in Fig. 7, in the order of type A, B and C. The first type A fracture seemed to be a fibre fracture. Next, the aspect changed to type B fracture, which included broad interfacial debonding. Finally, it developed into type C fracture in which the interphase was further debonded and the surrounding matrix distorted. It is still not certain whether these fractures mean fibre fracture, interfacial debonding or matrix distortion at this stage. This will be identified later by means of the finite element analysis.

Fig. 8 shows a plot of the number of fracture points versus crosshead displacement for non-surface treated specimen. The first fibre fracture occurred at displacement of around 3 mm. After the first fracture, the number increased with compressive loading.

5. Analytical results

5.1. Strain state in the macro model

The deformed shape of the macro model at a displacement of 3 mm is presented in Fig. 9. Matrix swelling at the central portion could be expressed theoretically as well as experimentally. The axial strain distribution within the macro model is shown in Fig. 10. A considerable strain concentration occurred at the centre-notched portion. Fig. 11 shows the relationship between the normal strain components of the central element and the applied displacement in the macro model. Each strain component proportionally increased after a displacement of 3 mm. The compressive strain along the Z axis, ε_{zz}, was the most considerable of the three components. Moreover, it was found that the ratio of ε_{xx}, ε_{yy} and ε_{zz} was almost constant, i.e. ε_{xx}: ε_{yy}: $\varepsilon_{zz} = 0.65 : 0.16 : 1.00$. The relationship can be used as input data for the micro model which incorporates fibre, interphase and matrix elements.

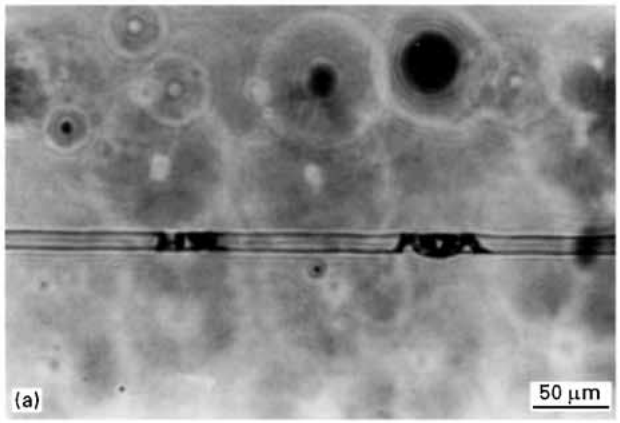

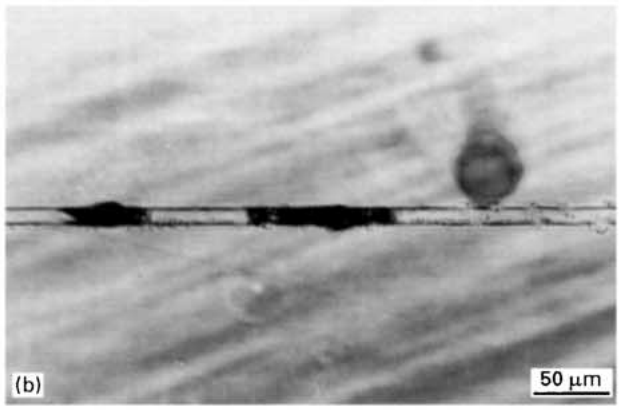

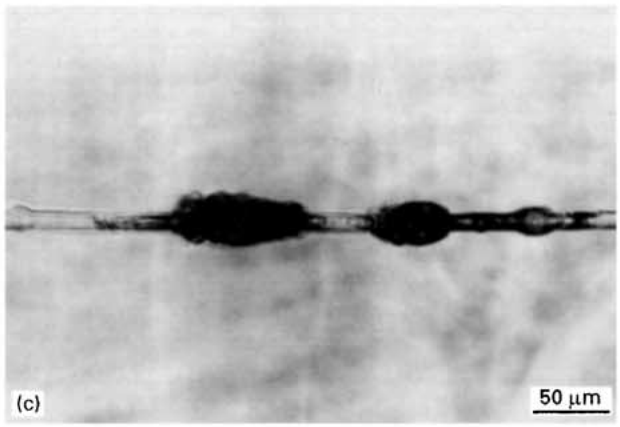

Figure 7 Fractures inside the single-fibre embedded compressive specimens. (a) A, (b) B, (c) C.

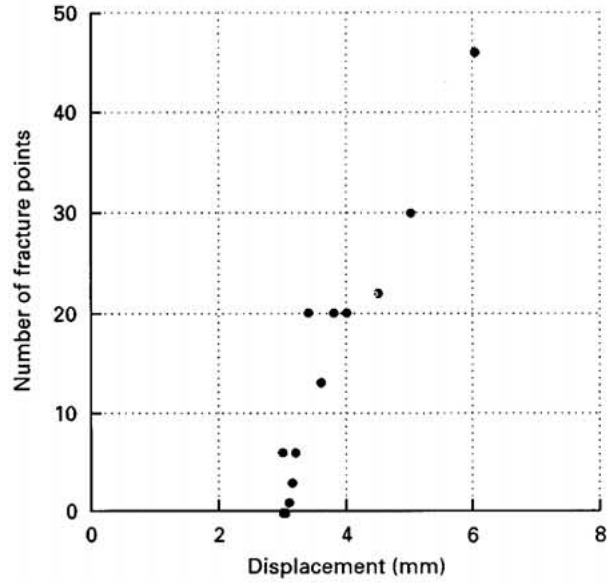

Figure 8 Plot of the number of fracture points versus displacement for non-APS treated specimen.

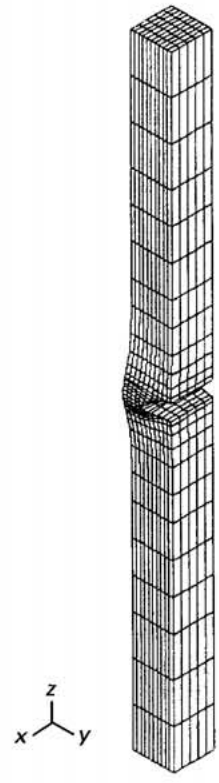

Figure 9 Deformed shape of the macro model.

5.2. Stress state in the micro model

Each strain ε_{xx}, ε_{yy} and ε_{zz} which satisfies the relationship obtained in the macro model was introduced into the matrix resin elements in the micro model. No strains were applied to the fibre and interphase elements because the deformation in this specimen was strongly concentrated in the particular notched region of the resin part, and progressively occurred from the outer surface. Therefore, it was assumed that the fibre strain was only the transmitted matrix strain through the interphase.

The analysis was separated into several steps as shown in Table IV. Step 6 corresponded to the displacement of 3 mm in the macro model. In the experiment, the first fibre fracture actually occurred around at this displacement level.

The interfacial modulus should be approximately determined for subsequent analysis here. Fig. 12 shows a plot of the normal stress along the fibre axis, σ_{zz}, in the bottom fibre element versus interfacial modulus at Step 6. Considering the compressive strengths of glass fibres obtained from the tensile recoil tests (1519–1922 MPa), the elastic modulus of interphase element should be approximately 10–30 GPa.

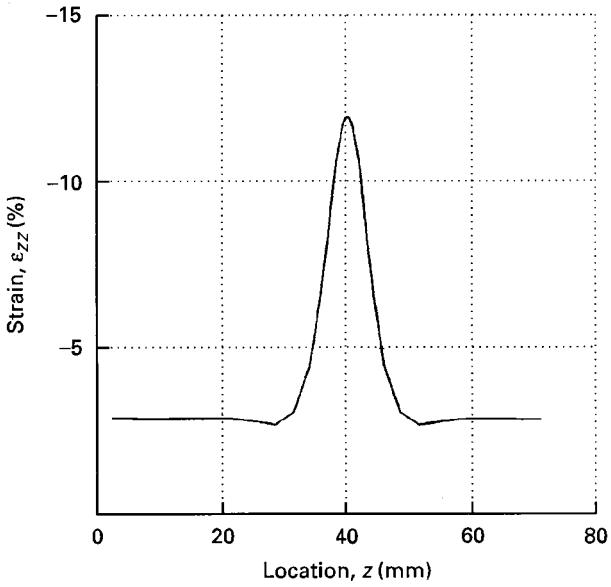

Figure 10 Axial strain distribution along the longitudinal direction.

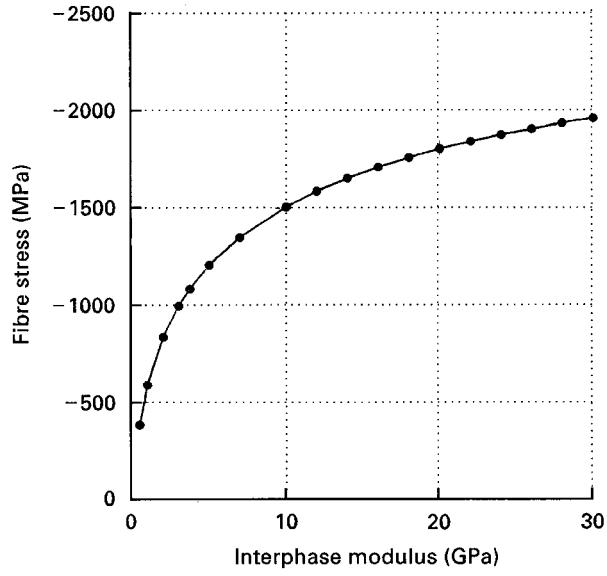

Figure 12 Relationship between the longitudinal stress in the bottom fibre element and the interphase modulus.

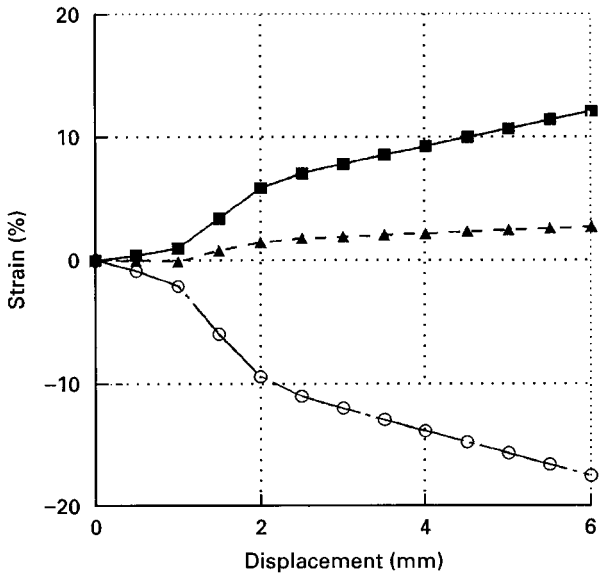

Figure 11 Relationship between strains of the centre element, $(X, Y, Z) = (0, 0, 40)$, and the applied displacement in the macro model. ε_{xx}: ε_{yy}: $\varepsilon_{zz} = 0.65 : 0.16 : 1.00$. (■) ε_{xx}, (▲) ε_{yy}, (○) ε_{zz}.

TABLE IV Input data increment in the analysis of the macro model and the micro model

Step	Applied displacement in the whole model (mm)	Applied strain components in the micro model (%)		
		ε_{xx}	ε_{yy}	ε_{zz}
1	0.5	1.28	0.32	− 1.95
2	1.0	2.61	0.65	− 3.98
3	1.5	3.91	0.97	− 5.97
4	2.0	5.22	1.29	− 7.95
5	2.5	6.52	1.61	− 9.94
6	3.0	7.83	1.94	− 11.93
7	4.0	10.44	2.58	− 15.91
8	5.0	13.05	3.23	− 19.88

As mentioned before, Step 6 in the micro model analysis corresponded to the displacement of 3 mm in which the first fibre fracture occurred. However, it is not still clear if this fracture really means fibre fracture; it could be interfacial debonding which occurred before any fibre fracture. In this case, the concept of the interfacial transmissibility is not applicable, because it aims to evaluate the interfacial property in the elastic range, without any damage to the interphase itself. We now need to investigate which component, fibre, matrix and interphase, first or subsequently fractured at the testing stage of the first fracture.

For this purpose, the analysis was broken down into three cases at Step 6. First, no fracture was supposed within the micro model (perfect model). Second, a fibre fracture occurs at Step 6 (fibre fracture model). Third, an interfacial fracture (debonding) occurs at Step 6 (interphase fracture model). Basically, each fracture was introduced in the bottom fibre or interphase element as shown in Fig. 13. The difference in stress states after Step 6 was the examined and compared for each fracture model. The elastic modulus of the interphase element was taken as 20 GPa.

Fig. 14 shows the change of von Mises equivalent stress in the bottom fibre element in each fracture model. In the prefect model, the equivalent stress increased until the end of the analysis. In the fibre fracture model, the equivalent stress did not increase after the bottom fibre fracture, because the bottom fibre element itself failed at Step 6. In the interphase fracture model, there was no change of the equivalent stress in the bottom fibre element at the Step 6. Fig. 15 shows the change of the equivalent stress in the bottom interphase element. In the fibre fracture model, the equivalent stress rapidly increased after the bottom fibre fracture at Step 6. In the interphase fracture model, there was no increase of the equivalent stress in the bottom interphase element, because the bottom interphase element itself failed at Step 6.

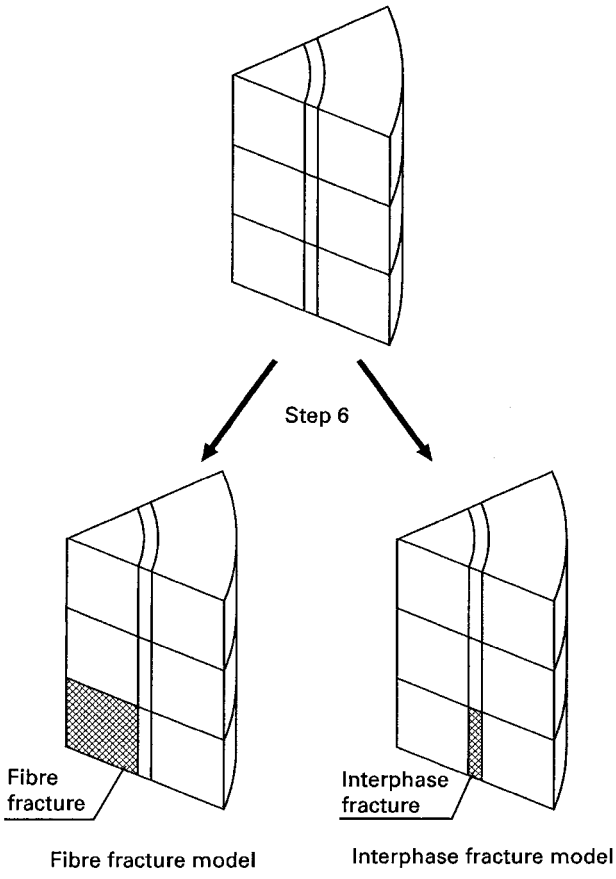

Figure 13 Location of fracture in each fracture model.

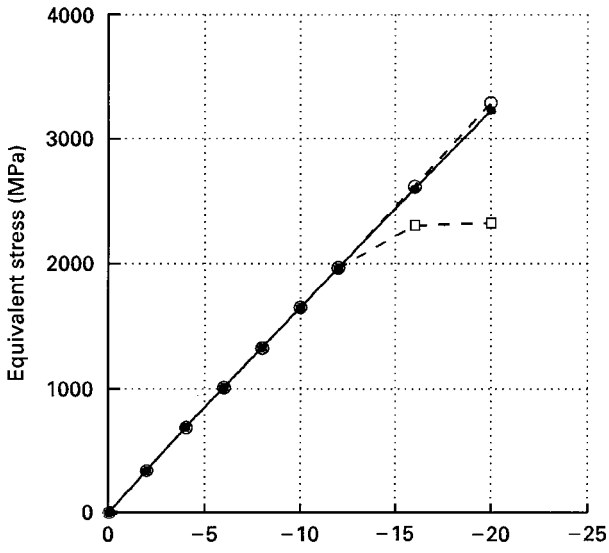

Figure 14 Change of equivalent stress in the bottom fibre element in each fracture model: (—●—) no fracture, (—□—) fibre fracture, (—○—) interphase fracture.

Changes in the equivalent stresses were similarly examined for other elements considering each fracture model. Summarizing the results, the change of stress state in each fracture model could be illustrated as shown in Fig. 16. In the fibre fracture model, the equivalent stress significantly increased in the bottom interphase and resin elements which were adjacent to the broken fibre element. Therefore, it is expected that

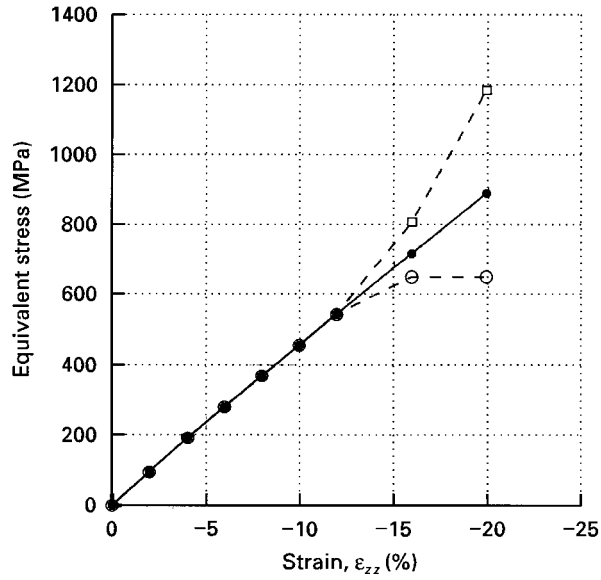

Figure 15 Change of equivalent stress in the bottom interphase element in each fracture model: (—●—) no fracture, (—□—) fibre fracture, (—○—) interphase fracture.

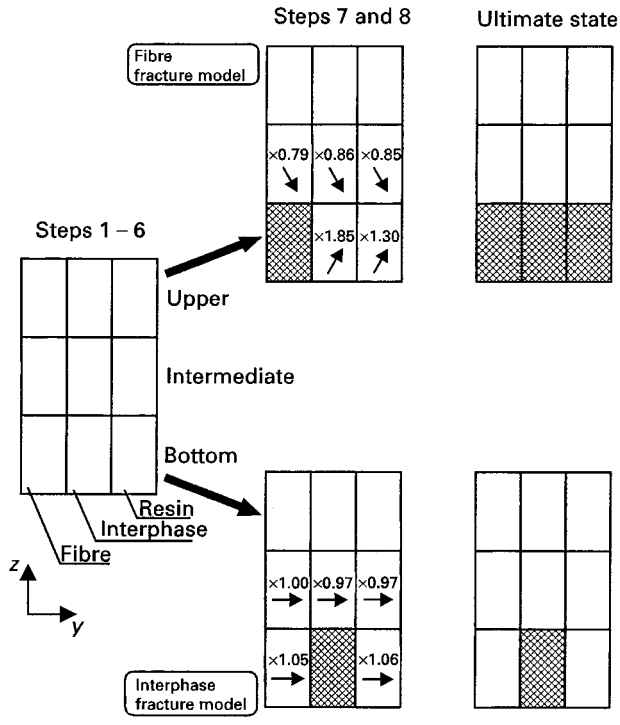

Figure 16 Expected failure state in each fracture model.

the bottom fibre, interphase and resin elements tend to fail at the ultimate stage. This tendency was quite similar to the experimental results, because the fibre fracture, interfacial debonding and matrix resin distortion occurred at the same position. On the other hand, in the interphase fracture model, there was no increase of equivalent stress in the surrounding elements. Therefore, the first interfacial debonding did not induce any fracture in the surrounding elements. This tendency was different from the experimental results.

From these analytical results, it was deduced that the assumption which supports the first fibre fracture

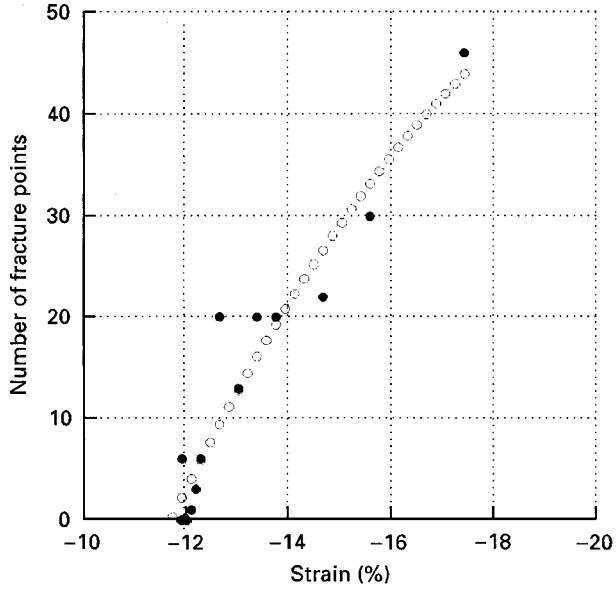

Figure 17 Plot of the number of fracture points versus strain for a non-APS treated specimen: (●) experiment, (○) best fit.

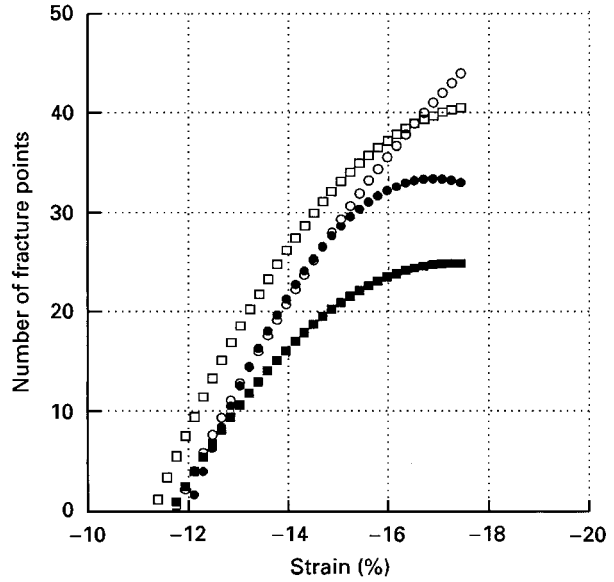

Figure 18 Best fit results of the relationships between the number of fracture points and strain. (○) No APS, (●) 0.1 wt % APS, (□) 0.5 wt %, (■) 1.0 wt % APS.

with elastic interphase is correct. The photographed type A, B and C aspects were probably fibre fracture, interfacial debonding and matrix distortion, respectively. Therefore, the evaluation of interfacial property based on the interfacial transmissibility was found to be applicable for the single-fibre embedded compressive tests conducted in this study.

5.3. Evaluation of the interfacial transmissibility

The number of the fibre fracture points observed in experiments was plotted against axial compressive strain obtained from the finite element analysis of the macro model. Fig. 17 shows a plot for non-surface treated fibre composites. Results were best fitted on to a two-dimensional function curve using the least-squares method. The best fit result for each treatment condition was compared in Fig. 18. It was seen that the first fibre fracture occurred at different strain for each case.

TABLE V Interfacial transmissibility for each surface treatment condition

Surface treatment condition	κ^a	ε_m^b (%)	σ_f^c (MPa)	E_f^d (GPa)
No APS	0.1629	11.72	1519	79.54
0.1 wt % APS	0.2299	12.00	1919	69.56
0.5 wt % APS	0.2196	11.29	1826	73.66
1.0 wt % APS	0.2156	11.65	1922	76.52

[a] $\kappa = \sigma_f/(E_f\varepsilon_m)$.
[b] ε_m = single fibre composite strain.
[c] σ_f = fibre compressive strength.
[d] E_f = fibre elastic modulus.

Interfacial transmissibilities calculated from Equation 4 are listed in Table V. It was found that the interfacial property was improved by the APS surface treatment agent and showed a maximum value for the 0.1 wt % APS treated specimen. Surface treatments with higher concentration resulted in rather lower interfacial properties.

6. Discussion

Glass fibre/epoxy resin interfacial properties were quantitatively estimated and compared by means of the interfacial transmissibility. The interfacial transmissibility showed the maximum value at 0.1 wt % APS treatment. Regarding to the tensile behaviour of the interphase in a similar composite system, Ikuta [53] obtained the maximum interfacial transmissibility for the 0.5 wt % treated specimen.

Ikuta proposed a reinforcing mechanism of the interphase based on the surface wettability theory, the chemical bonding theory and the deformable layer theory. At low concentrations of saline coupling treatment, physisorbed silanes enhance the interfacial transmissibility owing to the surface wettability effect. However, the interfacial transmissibility is not so high because the silane molecules are few at the low concentration. At intermediate concentrations, where the maximum interfacial transmissibility is obtained, the network structure of silanes is completed. The impregnation of the adjacent resin is thought to be excellent in this condition. The interfacial strength is improved because the rigid siloxane network and many of silane agents react with the matrix resin in such an interphase region, i.e. the chemical bonding theory. At high concentration, the thick interphase behaves like a deformable layer, which leads to rather low interfacial transmissibility. It is difficult for the matrix resin to impregnate the interphase network structure owing to the large thickness of the interphase. The matrix resin reacts with silane agents at outer side of the interphase, and the deformable behaviour of the interphase becomes significant.

The discrepancy of the maximum interfacial transmissibility between tension and compression states is

probably associated with the difference in the transverse stress within the interphase. In compression, a high transverse tensile stress occurs due to the plastic deformation of the specimen. During the compressive loading, the interphase could be thick due to the large Poisson's effect. Therefore, the interphase behaves like a deformable layer even at the intermediate concentrations of APS.

Thus, the results were strongly dependent on specimen geometry. However, it is valuable to evaluate and compare interfacial properties for different materials without any sophisticated apparatus under compressive loading.

7. Conclusion

Axial compressive strengths of single glass fibres were estimated by means of the tensile recoil method. It was found that the APS surface treatment agent could provide glass fibres with some coating effects and improve the compressive strengths.

The compressive behaviour of the interphase in the glass fibre/epoxy resin system was investigated by the single-fibre embedded compression technique. Quite unique fracture aspects of fibre, interphase and matrix were observed inside the specimen. Depending on the applied strain, the fracture aspects changed. Firstly, only fibre fracture occurred. Next, the interphase and matrix resin which was adjacent to the failed fibre, were distorted.

The interfacial property could be quantitatively evaluated as a parameter of interfacial transmissibility. It was confirmed that the interfacial property was improved by the surface treatment and the maximum adhesion was achieved in 0.1 wt % APS treated specimen. The result showed a discrepancy compared with that of the single-fibre embedded tensile test. This led to a problem with this method in which the result was dependent on specimen geometry; however, the comparison and qualitative discussion are still valuable for discussing various interphase conditions.

References

1. D. SINCLAIR, *J. Appl. Phys.* **21** (1950) 380.
2. J. H. GREENWOOD and P. G. ROSE, *J. Mater. Sci.* **9** (1974) 1809.
3. W. R. JONES and J. W. JOHNSON, *Carbon* **9** (1971) 645.
4. T. NORITA, A. KITANO and K. NOGUCHI, in "Proceedings of 4th Japan–US Conference on Composite Materials" (Techomic, Lancaster, PA, 1988) p. 548.
5. J. L. G. DASILVA and D. J. JOHNSON, *J. Mater. Sci.* **19** (1984) 3201.
6. E. TSUSHIMA, in "Proceedings of 34th International SAMPE Symposium", edited by G. A. Zakrzewski, D. Mazenko, S. T. Peters and C. D. Dean (SAMPE, Covina, CA, 1989) p. 2042.
7. S. J. DETERESA, S. R. ALLEN, R. J. FARRIS and R. S. PORTER, *J. Mater. Sci.* **19** (1984) 57.
8. S. J. DETERESA, R. S. PORTER and R. J. FARRIS, *ibid.* **23** (1988) 1886.
9. M. MIWA, T. OHSAWA, S. KAWAGUCHI, M. TSUSAKA, E. TSUSHIMA and J. TAKAYASU, *Sen-i Gakkai Preprints* (1990) S-248 (in Japanese).
10. H. M. HAWTHORNE and E. TEGHTSOONIAN, *J. Mater. Sci.* **10** (1975) 41.
11. D. J. BOLL, R. M. JENSEN, L. CORDNER and W. D. BASCOM, *J. Compos. Mater.* **24** (1990) 208.
12. M. MIWA, E. TSUSHIMA and J. TAKAYASU, *J. Appl. Polym. Sci.* **43** (1991) 1467.
13. J. R. WOOD, H. D. WAGNER and G. MAROM, *Adv. Compos. Lett.* **3**(4) (1994) 133.
14. L. DRZAL, Technical Report, AFWAL-TR-86-4003, Materials Laboratory, Air Force Wright Aeronautical Laboratories, Ohio, June 1986.
15. S. R. ALLEN, *J. Mater. Sci.* **22** (1987) 853.
16. M. G. DOBB, D. J. JOHNSON and C. R. PARK, *ibid.* **25** (1990) 829.
17. G. J. HAYES, D.D. EDIE and J. M. KENNEDY, *ibid.* **28** (1993) 3247.
18. C. S. WANG, S. J. BAI and B. P. RICE, in "Proceedings of the American Chemical Society", Vol. 61, Division of Polymeric Materials: Science and Engineering, Miami, FL, 1989 (ACS, 1989) p. 550.
19. M. FURUYAMA, M. HIGUCHI, K. KUBOMURA, H. SUNAGO, H. JIANG and S. KUMAR, *J. Mater. Sci.* **28** (1993) 1611.
20. L. GRESZCZUK, "Interfaces in Composites", STP **452** (American Society for Testing and Materials. Philadelphia, PA, 1969) p. 42.
21. M. P. PITKETHLY and J. B. DOBLE, in "Interfacial Phenomena in Composite Materials" (IPCM '89) edited by F. R. Jones (Butterworths Scientific, 1989) p. 35.
22. P. BARTOS, *J. Mater. Sci.* **15** (1980) 3122.
23. D. B. MARSHALL and W. C. OLIVER, *J. Am. Ceram. Soc.* **70** (1987) 542.
24. D. H. GRANDE, J. F. MANDELL and K. C. C. HONG, *J. Mater. Sci.* **23** (1988) 311.
25. T. WEIHS and W. NIX, *Scripta Metall.* **22** (1988) 271.
26. A. N. NETRAVALY, *Compos. Sci. Technol.* **34** (1989) 289.
27. L. T. DRZAL, in "Interfacial Behaviour of Aramid and Graphite Fibres in an Epoxy Matrix", 15th National SAMPE Technical Conference (1983) p. 190.
28. I. NARISAWA and H. OBA, *J. Mater. Sci.* **19** (1984) 1777.
29. N. IKUTA, Z. MAEKAWA, H. HAMADA, S. YOSHIOKA, E. NISHIO and T. HIRASHIMA, in "Interfaces in Polymer, Ceramic and Metal Composites", edited by H. Ishida, ICCI-II (Elsevier, New York, 1988) p. 611.
30. Z. MAEKAWA, H. HAMADA, S. YOSHIOKA, N. IKUTA, T. TANIMOTO and T. HIRASHIMA, *ibid.*, p. 553.
31. A. KELLY and W. R. TYSON, *J. Mech. Phys. Solids* **13** (1965) 329.
32. T. OHSAWA, A. NAKAYAMA, N. MIWA and A. HASEGAWA, *J. Appl. Polym. Sci.* **22** (1978) 3203.
33. M. MIWA and T. OHSAWA, *J. Mater. Sci.* **25** (1980) 795.
34. M. J. RICH and L. T. DRZAL, in "Proceedings of the 41st Annual Conference on Reinforced Plastics/Composites Institute SPI", Section 2-F (1986).
35. N. IKUTA, Z. MAEKAWA, H. HAMADA, H. ICHIHASHI and E. NISHIO, *J. mater. Sci.* **26** (1991) 4663.
36. H. HAMADA, Z. MAEKAWA, N. IKUTA, H. ICHIHASHI and E. NISHIO, in "Proceedings of the Japan–US CCM-V", A. Kobayashi, ed, Tokyo (1990) p. 535.
37. N. IKUTA, Z. MAEKAWA, H. HAMADA and S. YOSHIOKA, in "Proceedings of the Japan–US CCM-IV", Washington, DC (1988) p. 222.
38. T. LACROIX, B. TILMANS, R. KEUNINGS, M. DESAEGER and I. VERPOEST, *Compos. Sci. Technol.* **43** (1992) 379.
39. W. WU, M. DESAEGER, I. VERPOEST and J. VARNA, *ibid.* **57** (1997) 809.
40. D. TRIPATHI and F. R. JONES, *ibid.* **57** (1997) 925.
41. A. Di ANSELMO, M. L. ACCORSI and A. T. Di BENEDETTO, *ibid.* **44** (1992) 215.
42. Z. MAEKAWA, H. HAMADA, S. YOSHIOKA, N. IKUTA, T. TANIMOTO and T. HIRASHIMA, in "Interface in Polymer, Ceramic and Metal Matrix Composites", Proceedings of ICCI-II (Elsevier, New York, 1988).
43. A. N. GENT and C. J. WANG, *J. Mater. Sci.* **27** (1992) 2539.

44. P. A. KAKAVAS, N. K. ANIFANTIS, K. BAXEVANAKIS, D. E. KATSAREAS and G. C. PAPANICOLAOU, *ibid.* **30** (1995) 4541.
45. K. NISHIYABU, A. YOKOYAMA and H. HAMADA, *Compos. Sci. Tech.* **57** (1997) 1103.
46. B. FIEDLER and K. SCHULTE, *ibid.* **57** (1997) 859.
47. C. GALIOTIS and D. N. BATCHELDER, *J. Mater. Sci. Lett.* **7** (1988) 545.
48. A. PAIPETIS and C. GALIOTIS, *Compos. Sci. Technol.* **57** (1997) 827.
49. C. GALIOTIS, *ibid.* **48** (1993) 15.
50. N. MELANITIS, C. GALIOTIS, P. TETLOW and C. K. L. DAVIS, *J. Compos. Mater.* **26** (1992) 574.
51. M. C. ANDREWS and R. J. YOUNG, *J. Mater. Sci.* **30** (1995) 5607.
52. ASTM D695 "Standard Test Method for Compressive Properties of Rigid Plastics" (American Society for Testing and Materials, Philadelphia, PA).
53. N. IKUTA, "Study on Structure and Function of Interphase Treated with Silane Coupling Agents", Bulletin of Osaka Municipal Technical Research Institute, Vol. 92 (1991).

Received 4 November 1996
and accepted 22 April 1998